

Chapter 1

Introduction

As the communication technology advances, the demands for semiconductor devices performance for communication systems become more and more strict. Some of the requirements for the device performance is beyond what silicon industries can offer. We can expect that compound semiconductor will play more important roles in the future. The excellent properties of compound semiconductors such as easy to form ternary or quaternary heterostructures with same lattice constant, direct bandgap and high electron mobilities all make them suitable for optoelectronic and high speed device applications [1].

The heterojunction bipolar transistors (HBT) which is similar to bipolar junction transistor (BJT), with high electron mobility, built-in drift field, and velocity overshoot are traditionally made from AlGaAs/GaAs material system [2]. Although the AlGaAs/GaAs HBTs are superior to BJTs, there are many problems related to Al atoms included in the AlGaAs/GaAs material system. For example, the Al atoms are more sensitive to the traces of oxygen and humidity inside the reactor. The oxygen and humidity in the reactor will result in Al_2O_3 . This will greatly degrade the performance of the device. Besides, as the Al contentment of $\text{Al}_x\text{Ga}_{1-x}\text{As}$ increases above 0.45, the bandgap will change from direct to indirect. At this time, the deep level defect, DX center, will show up in the AlGaAs layer. These two major problems will deteriorate the performance of devices and make AlGaAs/GaAs material system

ineffective.

InGaP/GaAs material system is a good alternative to the original AlGaAs/GaAs material system for HBT applications [3]. There are many advantages of InGaP/GaAs. For example,

- (a) $\Delta E_g = 1.9$ eV: emitting light with $0.65\mu\text{m}$ wavelength (visible red light).
- (b) Large ΔE_v (0.24 eV): preventing the leakage hole-current from low band to high band.[4]
- (c) Low interface recombination velocity with GaAs: improving the minority carrier lifetime [5].
- (d) Insensitive to the traces of oxygen and humidity inside MOCVD reactor.
- (e) Free of DX center: no native deep donor trap defect [6].
- (f) High doping capability without creating deep levels defect.
- (g) High etching selectivity to GaAs: making process easy.

Figure 1.1 is the band diagram of InGaP/GaAs material system. The location of each alphabet represents the place of each advantage takes place.

According to the forementioned advantages, InGaP/GaAs material system seems to be unique for HBTs application. But there is a serious problem with the InGaP/GaAs material system. It is very hard for us to grow GaAs on InGaP with an abrupt interface.

As far as InGaP/GaAs material system is concerned, there are two kinds of InGaP/GaAs interfaces. One is InGaP on GaAs and the other is GaAs on InGaP. The former is so-called normal interface and is smooth. The latter is so-called inverted interface and is rough. Figure 1.2 shows

the schematic diagram of GaAs/InGaP/GaAs heterostructure interfaces. The study of T.K. Sharma *et al.* [7] shows a normal PL features corresponding to the band gaps of GaAs and InGaP for InGaP on GaAs, but an intense long-wavelength PL feature appeared as growing GaAs on InGaP while the features of InGaP and GaAs was suppressed [8-10]. The main reason for this difference is that the bonding strength between cations and anions of InGaP is weaker than that of GaAs. So as we grow GaAs on InGaP, the formation of intermixing $\text{In}_x\text{Ga}_{1-x}\text{As}_y\text{P}_{1-y}$ layer is spontaneous. Figure 1.3(a) is the diagram of GaAs/InGaP/GaAs heterostructure with an inserted $\text{In}_x\text{Ga}_{1-x}\text{As}_y\text{P}_{1-y}$ layer and Fig. 1.3(b) is the corresponding band diagram of Fig. 1.3(a). Judging from Fig. 1.3(b), we can see two reasons to explain why the PL features of InGaP and GaAs were suppressed:

(a) The GaAs and InGaP layers act as confined layer of $\text{In}_x\text{Ga}_{1-x}\text{As}_y\text{P}_{1-y}$ thus most of the holes and electrons will recombine within the $\text{In}_x\text{Ga}_{1-x}\text{As}_y\text{P}_{1-y}$ layer.

(b) Due to the formation mechanism of undesired $\text{In}_x\text{Ga}_{1-x}\text{As}_y\text{P}_{1-y}$ layer, the thickness of the $\text{In}_x\text{Ga}_{1-x}\text{As}_y\text{P}_{1-y}$ layer was about several nanometer. This enhances the quantum confinement effect.

Both of them will suppress the PL features of the GaAs and InGaP layers. In addition, according to the study of T. Nakano *et al.* [11], the desorption time of P from InGaP surface at 660°C was about 0.2 sec. So the desorption of P is too fast to grow an abrupt interface by MOCVD without forming InGaAsP intermixing layer. This will increase the roughness of GaAs/InGaP interface.

Roughness of the interface induces fluctuation in the energy level,

which in turn leads to the reduction of carrier mobility due to strong scattering and the broadening of the PL [12,13]. These are harmful to the InGaP/GaAs device properties. Here reducing the thickness of the InGaAsP intermixing layer is necessary for the growth of GaAs on InGaP.

Recently, InGaP was used as the etching stop layer between GaAs collector and subcollector for the InGaP/GaAs HBTs[14]. This etching stop layer will enhance the reproducibility and the reliability of the processes. Although InGaP has a high etching selectivity to GaAs, the spontaneously formed InGaAsP intermixing layer can be removed by the GaAs etching solution. This makes the required InGaP etching stop layer has to be thicker than traditional etching stop layer of other material systems, which is usually about $20\text{\AA} \sim 30\text{\AA}$. As the thickness of the InGaP etching stop layer increases, the performance of the HBT devices will deteriorate. This makes the growth of GaAs on InGaP without InGaAsP intermixing layer necessary.

This study will use different growth process to reduce the thickness of the InGaAsP intermixing layer, such as growth temperature and gas switching sequences to establish optimum growth conditions for the growth of GaAs on InGaP. Finally, we will use the optimum growth condition to grow a thin InGaP etching stop layer between GaAs and then examine the effect of the etching stop layer by performing carrying out the etching process in the heterostructure materials.

Chapter 2

MOCVD principle and system

MOCVD is a versatile growth technique for compound semiconductors. It can grow metals for IC fabrication and ferroelectrics for IC memory and optical applications [15]. Since the growth conditions for MOCVD are far from equilibrium, stable and meta-stable compounds can be grown. Thus almost any combinations of layers and layer sequences can be deposited on almost any crystalline substrates and this makes the band gap engineering become practical [16]. We can select many different compounds or layer sequences to modulate the ΔE_v and ΔE_c of the devices to enhance the device performance. But when the thickness of the deposited layer is thicker than critical thickness, the strain due to lattice constant mismatch must be relaxed by crystal defects such as dislocations and microtwins.

Thermodynamics, fluid dynamics, gas types, and surface reactions play important roles in the MOCVD deposition process at different temperature range [17]. The growth mechanism can be determined by control of external process parameters, such as growth rate, substrate temperature and input precursor flow rates. The design of the MOCVD system also has great influence on the epitaxial quality, such as reactor chamber, gas handling system, heating system, *etc.* Careful control of growth parameters and gas switching sequences during deposition process will result in good epitaxial quality.

2-1 Principle of MOCVD

The fundamental principles of MOCVD include the chemistry of the source molecules, which are so-called precursors, the thermodynamics and kinetics of the processes, mass transport and growth processes.

Figure 2.1 is a typical reciprocal temperature *versus* growth rate curve for MOCVD processes. Usually three regimes are distinguishable [18]. The growth process is thermally activated at temperature below 550°C where the growth rate increases exponentially with temperature. Here the layer quality tends to deteriorate. This is kinetic controlled regime. Usually an intermediate temperature range exists between 550°C ~ 750°C, in which the rate is independent of temperature and is determined by the supply of source materials diffusing through the boundary layer to the surface. Under most conditions this process is governed by the diffusion of the group III species and thus is called the diffusion or transport controlled growth regime. As temperature above about 750°C, the rate may drop again due to the desorption of the reactants, almost the group V elements, from the surface or enhanced parasitic pre-reactions, which may lead to a significant depletion of the precursor concentration along the substrate holder resulting in inhomogeneous growth and deteriorate the quality of deposited layer and this is called the thermodynamic controls regime.

In addition to the three growth mechanisms, precursor properties such as saturation vapor pressure and relation between pyrolysis efficiency and temperature also play important roles during MOCVD process.

2-1-1 Precursor properties

Many characteristics of the MOCVD growth process and properties of the resulting materials are determined by the nature of the precursor molecules [15]. Besides, in order to complete various material combinations, we must develop the high degree of flexibility in the design of precursor molecules. In general, we use metalorganic compounds as group III precursors and hydrides as group V precursors.

a. Group III precursors

Metal-organic chemical vapor deposition is a form of CVD utilizing metalorganic compounds for one or more of the precursors. The normally widely used metalorganic compounds are the methyl and ethyl compounds of the group III metal shown in table 2.1. Due to the lower and reasonable vapor pressure at room temperature of group III precursors, they are only useful in LP-MOCVD. A clear trend of increasing stability of the precursors with the progression from In to Ga and Al is observed. In addition, as the carbon length of group III increases, the vapor pressure of the precursors will decrease at the same temperature. Besides, the CH_3 radicals produced from group III precursors can lose hydrogen in the process, resulting in highly reactive CH_2 that may decomposed and produce C contamination in the epitaxial layer. A more rapid way to remove CH_3 is by reacting with atomic H on the surface by pyrolysis of the group V precursor. Table 2.1 shows the methyl and ethyl compounds of the group III metals. It has be seen that TMIIn is solid form at room temperature, so it is hard to make sure that the carrier gas flowing out of the TMIIn stainless steel bubbler is saturated with the TMIIn vapor.

The best way is to make two or more TMIn stainless steel bubblers in series connection, to solve this problem. In addition, the saturation vapor pressure (P) can be driven from the following equation:

$$\text{Log}P[\text{Torr}] = A - (B/T) \quad T : \text{absolute temperature}$$

A and B are constant.

In our experiments, we choose TEGa and TMIn as the group III precursors. Figures 2.2 and 2.3 show the pyrolysis curves of TEGa and TMIn in different carrier gases, respectively. Judging from the diagram, it can be found that TEGa and TMIn decompose completely at the deposition temperature used in this work, *i.e.*, 575°C to 650°C. Table 2.1 also shows the saturated vapor pressure of each precursor at 15°C which is the temperature we chose to keep our stainless steel bubbler in the bath tank.

b. Group V precursors

The hydrides, AsH₃ and PH₃, serves as the Group V precursors. Because of the higher vapor pressure of Group V precursors, the hydrides are used in excessive supply to prevent the desorption of the group V species from the solid-gas interface, so the deposition procedure is carried out at a high V/III ratio ambient. The H radicals from group V precursors on the surface lead to the removal of the C radicals generated from pyrolysis of the common group III precursors, thus the C contamination can be reduced. Although group V hydrides have such attractive properties, there is a serious problem to use them as precursors due to their highly toxicity. The threshold limit values for AsH₃ and PH₃ are 0.05 ppm and 0.03 ppm, respectively [17]. Threshold limit value is

the maximum permissible exposure limit based on a time-weighted average for an 8-h day.

Figure 2.4 is the percentage decomposition *versus* temperature for 5% concentration of AsH₃ in various ambient at different surfaces according to the Larsen's study. From this reference, we can find that the temperature at which pyrolysis is 50% complete, T₅₀, for a residence time of 4 sec is approximately 476°C for GaAs surfaces. Figure 2.5 is the dependence of the PH₃ pyrolysis on different carrier gases and surface types. Curve *A* is of the same reacting tube, 60 cm², but with different carrier gases such as N₂, H₂ and D₂. Curve *B* has the same carrier gas, D₂, as Curve *A* but pyrolysis is performed in a bigger reacting tube, 300 cm². Curve *C* has the same carrier gas and tube size as Curve *A* but with InP coating on the tube wall. We can draw the following conclusion from Figs. 2.4 and 2.5, carrier gas type has no influence on the decomposition process, however, parameters such as temperature, chamber size and reacting surface all play important roles during the pyrolysis process. In addition, PH₃ is more difficult to decompose than AsH₃ at the same temperature and this leads to higher growth temperature when PH₃ precursor was used, therefore, the range of the growth temperature is frequently limited by the pyrolysis process of the precursors.

2-1-2 Thermodynamics

The epitaxial growth is simply a highly controlled phase transitions, it contains the pyrolysis of the gas phase and the formation of the solid phase. During these processes, thermodynamic determines the driving force for the overall growth conditions. As far as MOCVD growth

process is concerned, it is far from thermodynamic equilibrium. Thus, thermodynamics defines only certain limits for the growth process, for example, the driving force, maximum growth rate, number and compositions of the equilibrium phases in the bulk or on the surface. We can only determine which process will occur at different temperature and pressure from thermodynamic calculation. This helps us to understand the complex process of MOCVD deposition.

2-1-3 Kinetics

Although thermodynamics deals with the energy of the system in the initial and final equilibrium states, it is unable to provide any information about the time required to attain equilibrium. Especially at very low temperature, the growth process is too slow to be determined from the thermodynamic equilibrium approximation. The chemical reactions, homogeneous reactions which occurs in the gas phase and heterogeneous reactions which occurs on the surface, determine the growth process. At this time we must use kinetics to determine the rates of various steps.

2-1-4 Hydrodynamics and mass transport

Hydrodynamics determines the boundary layers, dead regions and the temperature profile near the heated substrate. Since gas phase diffusion is a temperature independent process, the growth rate is nearly independent of substrate temperature in the mass transport limited case. But the growth rate is linear dependent of group III flow rate in the temperature range where mass transport is the growth rate determining step in the

overall process. This suggests that the group III molecules are completely depleted at the solid-vapor interface. The overall MOCVD growth process is schematically illustrated in Fig. 2.6. There is a boundary layer formed spontaneously. The thickness of the boundary layer is related with the shape of the reactor chamber and the flow velocity of the gas. It can be derived from the following equation:

$$\delta \propto (x^2/R_e)^{1/2}$$

δ : Thickness of the boundary layer

x : Gas flowing distance from the wafer edge

R_e : Reynolds number

Usually III-V semiconductor are grown in the diffusion controlled (transport limited) regime. In this temperature regime small variation in temperature have no influences on the layer properties. In the diffusion controlled regime the growth rate, r_g , is linearly proportional to the molar flow of the group III species and can be evaluated with the following equation[18,19] :

$$r_g = (constant) P_{III} * (v/p_{tot})^{1/2}$$

P_{III} : The group III partial pressure

p_{tot} : The total reactor pressure.

v : The gas velocity

2-2 Description of MOCVD system

Generally speaking, the MOCVD system contains several important parts. These are bubbler system, gas switching system, reacting chamber,

pumping system, gas purifying system, exhaust system and safety apparatus. These are different from each manufacturer [20]. As to our MOCVD system, it is a self-assembled system. Figure 2.7 is the schematic diagram of our MOCVD system. We will describe our MOCVD system here and some growth parameters during MOCVD deposition process as follows.

2-2-1 Reactor chamber

The growth process is influenced by the reactor design. The presence of vortices and dead volumes (sharp corners in reactor inlet) will act as sources of undesired materials that are hard to remove completely and will cause undesired reactions. Therefore, the smoothness of the reactor shape and well designed reactor can eliminate the undesired reaction. Currently, the horizontal low pressure reactor and the high speed rotation disk reactor are popular for the deposition of high quality uniform films for a variety of materials [15]. Cold wall is typically used for MOCVD to prevent the contamination from chamber wall. The apparatus we used is a horizontal reactor with a hot wall chamber. The reactor vessel is a rectangular quartz tube with 2-inch wafer susceptor. Our reactor is made from fused silica because of its chemical inertness, optical transparency and low electrical conductivity. And the susceptor is made of graphite. Figure 2.8 is the schematic diagram of our reactor system and the geometry of reactor and susceptor.

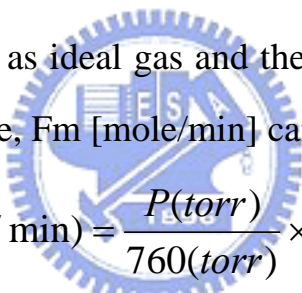
2-2-2 Gas handling system

The gas handling system contains sources of alkyls and hydrides stainless steel bubblers, manifold, mass flow controller (MFC), electrical pressure control (EPC), and different kinds of pumps. The most important

function of gas handling system is to deliver the reacting gas to the reactor chamber with precise amount at accurate time.

a. Stainless steel bubblers

Most metalorganic are highly reactive with oxygen so they are contained in stainless steel bubblers and met he carefully handled to avoid their contamination by air. Generally, the stainless steel bubblers are immersed at a bath tank at fixed temperature. In addition, the metalorganic compounds which kept at a constant temperature and therefore a constant vapor pressure. Figure 2.9 is the schematic diagram of the bubbler and bath tank. Here, H₂ serves as carrier gas to carrier the metalorganic vapor into the reactor. In the following equation, the vapor of the precursor is treated as ideal gas and the approximate evaluation of precursor's molar flow rate, F_m [mole/min] can be obtained by


$$F_m(\text{mole / min}) = \frac{P(\text{torr})}{760(\text{torr})} \times \frac{F_v(\text{sccm})}{22400(\text{c.c.})}$$

P : vapor pressure of reactant

F_v :flow rate of hydrogen

b. Electronic mass flow controllers

As the carrier gas delivering the MOCVD precursors to reactor chamber, the mass flow controller is utilized to accurately control the mass flow rate of the carrier gases.

c. Manifold

Before gas source flow reaches the reactor chamber, a manifold is used to determine which types of the source gases should enter the reactor or bypass to the exhaust system.

2-2-3 Heating System

There are three types of the heating method to heat the susceptor: radio frequency (RF) induction heating, radiative heating and resistance heating. Our system uses the RF induction heating. In our RF heating, the graphite susceptor is inductively coupled to the RF coil. This type of heating is used for large industrial reactors.

2-2-4 The growth parameters in MOCVD

There are many characteristic growth parameters in MOCVD. Table 2.2 lists the growth parameters. These parameters have important influences on the uniformity of the composition, thickness and carrier concentration of the film deposited. They also affect the photoelectrical properties and the interface properties of the epitaxial structure. In the following paragraph, we will discuss some of these growth parameters which are important to the growth process.

a. The growth temperature

The growth temperature (T_g) is the most important parameter in MOCVD. As discussed previously, most of the MOCVD deposition processes are carried out in mass transport control regime at $550^{\circ}\text{C} \sim 750^{\circ}\text{C}$. When the growth temperatures are below this range, 3-dimension growth occurs and it will destroy the surface morphology. When the growth temperatures are higher than these temperatures, the deposited layer is easy to have high carbon incorporation. Therefore there is an optimum growth temperature for various materials. In our study, we grow GaAs at 575°C , 600°C , 625°C , 650°C and InGaP at 650°C .

b. The pressure of growth chamber

Table 2.3 shows the requirements for the atmospheric pressure growth process. The low-pressure MOCVD (LP-MOCVD) can reach this objective. According to C.Y. Chang's study [21], the lower reactor pressure improved the uniformity of epi-layer. As the growth pressure decreased, the diffusion coefficient increased, thus, the mass transport rate increased. Another advantage for the LP-MOCVD is the enhancement of the homogeneity, reduction of the undesired gas phase reactions [22], reduction of out-diffusion and auto-doping, and the improvement of the interface sharpness and the doping profiles, lower growth temperature, improving thickness uniformity and compositional homogeneity and eliminating the memory effects [23,24]. The disadvantage of low growth pressure is that the decomposition of the precursors is reduced and a higher V/III ratio is necessary.

c. The V/III, III/III and V/V ratio

The V/III ratio is obtained from following equation:

$$V/III = [\text{Hydride}] / [\text{Alkyl}]$$

Taking GaAs as an example, the V/III ratio is $[\text{AsH}_3] / [\text{TEGa}]$. Because the group V elements are volatile at general growth temperatures, the growth processes are carried out in group V element rich ambience. If the V/III ratio is not large enough, it will cause the formation of group V vacancy and deteriorate the surface morphologies.

For ternary or quaternary systems, the III/III and V/V ratios are very important too. Taking InGaP as an example, the $[\text{TEGa}] / [\text{TMIIn}]$ ratio will determine the composition of InGaP ternary compound. As we

known, the energy gap, lattice constant, and electron mobility vary with the composition. So when growing ternary or quaternary compound semiconductors, we must choose the proper III/III and V/V ratios to achieve the objectives.



Chapter 3

GaAs/InGaP Heterostructure Characterization

As mentioned previously, InGaP/GaAs is an attractive alternative to traditional AlGaAs/GaAs system for application to heterojunction bipolar transistors and high electron mobility transistors (HEMT) [25]. Lattice matched InGaP has a direct band gap of 1.9 eV (0.65 μm), which is equivalent to the maximum direct band of AlGaAs [26]. InGaP is free of DX centers, which effectively reduce the free electron concentration in AlGaAs [27]. It is also insensitive to the traces of oxygen and humidity inside the MOCVD reactor. Nevertheless, InGaP possesses several problems, difficulties including the existence of ordered/disordered phases and the exact composition control. The former results in the reduction of the band gap up to 100 meV. The latter increases the difficulty to grow InGaP with lattice match to GaAs. In addition, it is hard for us to grow GaAs on InGaP with abrupt and smooth interface due to the interdiffusion of As and P atoms.

3-1 InGaP properties

The energy gap of $\text{In}_x\text{Ga}_{1-x}\text{P}$, varies with the compositions of group III atoms. When the composition of Ga is higher than 0.74, $\text{In}_x\text{Ga}_{1-x}\text{P}$ transfers from direct bandgap to indirect bandgap and creates lot of DX-centres. Nelson and Holonyak found the formula between energy band gap and composition of $\text{In}_x\text{Ga}_{1-x}\text{P}$ [28] as

$$E_g (300\text{K}) = 1.351 + 0.73x + 0.70x^2$$

In addition, $\text{In}_x\text{Ga}_{1-x}\text{P}$ has order or disorder structures and both exhibit a high etching selectivity to GaAs. As growing with GaAs, different growing sequence will result in normal (InGaP/GaAs) or inverted interface (GaAs/InGaP). These characteristics make $\text{In}_x\text{Ga}_{1-x}\text{P}$ a particular material for us to use.

3-1-1 Ordering and disordering structures

In the $\text{In}_x\text{Ga}_{1-x}\text{P}$ ordered structure, the cations are not randomly distributed, but occupy alternate (111) plane giving a spontaneous CuPt-type structure in the group III sublattice [26]. Figure 3.1(a) is the CuPt-type, Fig 3.1(b) is the 2-D and Fig. 3.1(c) is the 3D diagram of ordering $\text{In}_x\text{Ga}_{1-x}\text{P}$. The consequence of ordering is that the crystal symmetry is lowered in the $\langle 111 \rangle$ directions.

3-1-2 Ordering formation mechanism

The driving force for the ordering process is the reducing of strain energy resulting from the large difference in the lattice parameters of GaP and InP [29]. The CuPt-type ordering is the most common ordering structure in MOCVD grown III-V alloys with a peculiar dependence on the growth parameters such as growth temperature, III/V ratio, growth rate, and doping [30]. As $\text{In}_x\text{Ga}_{1-x}\text{P}$ is concerned, the critical parameter to cause ordering structure is temperature. Generally speaking, the degree of ordering reach the maximum at 650°C .

3-1-3 Characteristics related to ordering

The ordering effect results in a reduction of the band gap up to 100 meV for a fixed composition [31-34] and affects the spectra measured by reflectance anisotropy spectroscopy [35,36]. It also shows anisotropic bulk properties. On the other hand, the minority carrier lifetime is severely affected by this cation ordering [33].

3-2 Characteristics of GaAs/InGaP heterostructure

As discussed in Ch.1, according to T.K. Sharma's study [7], normal PL features corresponding to the band gaps of GaAs(820 nm) and InGaP(644 nm) are usually seen for InGaP layer grown on GaAs (This is denominated spectra for the normal interface). However, an intense long-wave length PL feature was observed if GaAs were grown on InGaP (This is denominated by the inverted interface) while the features of InGaP and GaAs are suppressed. This PL feature varies significantly in wavelength with changes in the switching sequence. This result comes from the formation of $\text{In}_x\text{Ga}_{1-x}\text{As}_y\text{P}_{1-y}$ intermixing layer between GaAs and InGaP. Because the value of x and y varies with different growth condition, the PL features of $\text{In}_x\text{Ga}_{1-x}\text{As}_y\text{P}_{1-y}$ change. In addition, growth of abrupt GaAs/InGaP heterjunction with an abrupt interface by MOCVD has been proved to be difficult because the intermixing of arsenic and phosphorus at the heterointerface [37 - 40] and the In memory effect [41,42].

3-2-1 Growth of InGaP with lattice matched with GaAs

$\text{In}_x\text{Ga}_{1-x}\text{P}$ matches the GaAs lattice when $x = 0.516$ at room temperature. However, due to the large lattice mismatch among InP, GaP and GaAs, the adjusting of the composition is critical to avoid strain in the layers. Even a small deviations from $x = 0.516$ can induce large lattice distortions [43]. To grow $\text{In}_x\text{Ga}_{1-x}\text{P}$ with lattice matching with GaAs, the $[\text{TEGa}] / [\text{TMIIn}]$ ratio is very important. It determines the x value of $\text{In}_x\text{Ga}_{1-x}\text{P}$. Because the pyrolysis temperature of TEGa and TMIIn is different, the $[\text{TEGa}] / [\text{TMIIn}]$ ratio is not the same for different growth temperature. For different growth temperature, there is an different optimum $[\text{TEGa}] / [\text{TMIIn}]$ ratio that makes x equal to 0.516.

3-2-2 Formation of $\text{In}_x\text{Ga}_{1-x}\text{As}_y\text{P}_{1-y}$ at the interface of GaAs/InGaP

It is difficult to grow sharp GaAs/InGaP interfaces because of the exchange and diffusion processes in the group V sublattice which results in the formation of $\text{In}_x\text{Ga}_{1-x}\text{As}_y\text{P}_{1-y}$ layer between GaAs and InGaP. To achieve a sharp interface, a monolayer P-atom must be followed by a pure monolayer As-atom without exchanging in the group V sublattice. This is extremely difficult due to the low binding energy of the group V elements on the InGaP surface [44]. As we grow GaAs on InGaP, the P atoms of InGaP will desorb during PH_3 off step and the As atoms will diffuse into the InGaP layer and occupy the original P lattice sites. It has been speculated that the $\text{In}_x\text{Ga}_{1-x}\text{As}_y\text{P}_{1-y}$ layer may be formed either by (i) the displacement of P by As when arsine is introduced to grow GaAs [38 - 40] or, by (ii) the motion of In from the ambient or from the underlying InGaP [41, 42]. As to our experiment, we believed the exchange process

to be the mechanism of $\text{In}_x\text{Ga}_{1-x}\text{As}_y\text{P}_{1-y}$ formation. We will discuss the reasons in the following paragraph.

3-2-3 Characteristics related to the InGaAsP layers between GaAs and InGaP

The overall quality of the GaAs/InGaP system is strongly influenced by the quality of the interfaces. The desorption of P and the adsorption of As during the formation of the interfaces reduce the abruptness of P to As composition [11]. This has great influences on the optical and electronic properties. In addition, the observed long-wavelength PL is resulted from the formation of $\text{In}_x\text{Ga}_{1-x}\text{As}_y\text{P}_{1-y}$ layer during the growth of GaAs on InGaP.



3-3 Use of InGaP as GaAs/InGaP/GaAs HBT subcollector etching stop

According to Fig. 1.1, the GaAs/InGaP system with small conduction band and large valance band discontinuities is chosen to support carrier tunneling and hole confinement. Modern GaAs/InGaP HBTs with an InGaP etch-stop between the lightly doped collector and the heavily doped subcollector enables a more robust processing. It ensures a flatter surface for the collector metal to be deposited than a conventional structure without an etching stop layer [14]. Figure 3.2 is the energy band diagram of the base-collector junction of InGaP/GaAs HBT. There is one conduction spike between GaAs collector and the

InGaP etching stop and one between the InGaP etching stop and the GaAs subcollector. These spikes are barrier for the motion of electrons. Due to the spontaneous intermixing process between GaAs and InGaP, the InGaP etching stop layer includes some InGaAsP intermixing layers. The thickness of the InGaAsP intermixing layers are closely dependent on the growth process and can be removed by the etching solution of the GaAs. So the required thickness of the InGaP etching stop of the GaAs/InGaP material system is thicker than the traditional etching stop layer of other material systems. As the thickness of InGaP etching stop layer increases, the electronic tunneling effect will be restrained and the band bending will become obvious. It results in the increase of the resistance. So it is attractive to reduce the thickness of the InGaP etching stop layer while using InGaP as GaAs/InGaP/GaAs HBT subcollector etching stop.



Chapter 4

Experiment

As mentioned previously, the epitaxy layer in this study was grown by a home-made MOCVD system with the horizontal quartz reactor which is kept at 40 torr by a computer controlled throttle valve. TEGa and TMIn were used as group III precursors and both of them are kept in a bath tank at 15°C. AsH₃ and PH₃ were used as group V precursors. Figure 4.1 is the schematic layer structures of our MOCVD samples grown in this study. The deposition processes are carried out on the (001) semi-insulator GaAs substrates. The temperature of the reactor was controlled by a RF heating system and the growth temperatures of our experiment were 650°C for InGaP, 620°C for GaAs buffer, and 575°C, 600°C, 625°C and 650°C for GaAs cap layers, respectively. The III/V ratio was about 125 for GaAs and 185 for InGaP. The [TEGa]/[TMIn] ratio for InGaP was about 1.68. We used H₂ as the carrier gas to deliver source molecules into the reactor chamber and baked our substrate at 700°C to clean the surface. After baking, we grew GaAs buffer, InGaP layer and GaAs cap layer at temperatures described above. A proper PH₃ off time is necessary during the growth of GaAs on InGaP. If the PH₃ off time were too short, the residual PH₃ cannot be completely removed out of the reactor chamber. If the PH₃ off time were too long, it would cause the desorption of P atoms from the InGaP surface. Both of them would

result the formation of InGaAsP intermixing layer. We inserted a 1 second PH₃ off time between InGaP and GaAs with different GaAs growth temperatures at first. After we found the optimum growth temperature for GaAs cap, we used different PH₃ off time to reduce the thickness of the InGaAsP intermixing layer. After all these have been done, we used the optimum growth condition to grow the thinnest InGaAsP intermixing layer and several samples with different thickness of the InGaP layer between GaAs as etching stop layer. Finally, we examined the quality of our InGaP etching stop layer by mesa etching. Figure 4.2 is our experimental flow chart.

4-1 InGaP /GaAs heterostructure growth

There are two major problems during InGaP/GaAs heterostructure growth, one is the growth of lattice-matched InGaP on GaAs substrate and the other is the native interface roughness as growing GaAs on InGaP. These are two major difficulties we attempted to overcome in this study.

4-1-1 Growth of InGaP lattice matched with GaAs substrate

Due to the large lattice mismatched between InP, GaP and GaAs, the composition of In_xGa_{1-x}P whose lattice matches with GaAs must be defined exactly. As mention previously, In_xGa_{1-x}P lattice matches with GaAs when $x = 0.516$. In our study, we kept a constant flow rate of TEGa and changed the TMIn flow rate to modify the III/III ratio. This changed the x -value of In_xGa_{1-x}P. According to the data of double crystal x -ray (DCX) of different samples, we modified the TMIn flow rate to optimize

the lattice match of the $\text{In}_x\text{Ga}_{1-x}\text{P}$ on GaAs substrate.

4-1-2 Growth of GaAs cap on InGaP

The most important process of this study is to eliminate the intermixing $\text{In}_x\text{Ga}_{1-x}\text{As}_y\text{P}_{1-y}$ layer between GaAs and InGaP. The formation of $\text{In}_x\text{Ga}_{1-x}\text{As}_y\text{P}_{1-y}$ is irremediable but we can utilize some parameters to reduce the thickness of the $\text{In}_x\text{Ga}_{1-x}\text{As}_y\text{P}_{1-y}$ layer. The PH_3 off time between GaAs cap and InGaP is an ordinary experimental parameter. The difference between our experiment and others is the GaAs cap growth process. Generally, the growth temperature of GaAs cap and InGaP layer is the same. Due to the fact that PH_3 is hard to decompose, higher growth temperature for InGaP is required. The best growth temperature for InGaP growth is between $640^\circ\text{C} \sim 670^\circ\text{C}$ [31]. We grew InGaP at 650°C and change the growth temperature of GaAs cap to 625°C , 600°C and 575°C . This was to reduce the desorption of P atoms from InGaP and helped to eliminate the intermixing of the $\text{In}_x\text{Ga}_{1-x}\text{As}_y\text{P}_{1-y}$ layer. As expected, the optimum growth temperature of GaAs cap was 575°C according to the PL data. Subsequently, the GaAs cap was grown at 575°C and the insert different PH_3 off time of 0 sec, 1 sec, 2 sec, 3 sec and 10 sec were evaluated respectively.

The DCX, PL, TEM and STEM were used to examine the quality of the epitaxial layers and the intermixing $\text{In}_x\text{Ga}_{1-x}\text{As}_y\text{P}_{1-y}$ layer.

4-1-3 Use of InGaP as GaAs/InGaP/GaAs etching stop

The final goal of our study is to grow a thin InGaP etching stop layer within a thinnest InGaAsP intermixing layer between InGaP at GaAs

layers. The mesa etching was performed to examine the quality of the thin InGaP layer grown and was accomplished by employing the $\text{H}_3\text{PO}_4:\text{H}_2\text{O}_2:\text{H}_2\text{O} = 1:1:20$ solution. This etching solution will remove GaAs and intermixing InGaAsP layers. If the undesired InGaAsP is the majority of InGaP layer, the InGaP layer would be penetrated and could not prevent the sub-GaAs from being etched. The InGaP etching stop layer with different thickness were grown and evaluated to obtain the thinnest InGaP etching stop layer. After mesa etching, we used P-10 to measure the depth profile and to verify if the etching stop layer was penetrated.

4-2 Heterostructure properties measurement

4-2-1 Use of DCX diffraction to evaluate lattice mismatch of InGaP on GaAs substrate

The analysis of the data of DCX is based on the Bragg's law. Angular positions of the Bragg peaks of the epilayers and substrates are related to the lattice constant of the material. The formula of Bragg's law is:

$$2d \sin \theta_B = n \lambda \quad n = 1, 2, 3, \dots$$

λ : x-ray wavelength

From the angular position of the substrate and the epilayers, we can calculate the lattice mismatch value, $\Delta a/a$, and determine the lattice constant of $\text{In}_x\text{Ga}_{1-x}\text{P}$ grown. Finally, the alloy composition of the ternary alloy can be determined from the lattice constant by using Vegard's law.

Taking $\text{In}_x\text{Ga}_{1-x}\text{P}$ for example, the lattice constant of $\text{In}_x\text{Ga}_{1-x}\text{P}$ can obtain from the following equation:

$$d_{\text{In}_x\text{Ga}_{1-x}\text{P}} = xd_{\text{InP}} + (1-x)d_{\text{GaP}}$$

In addition, the full width at half maximum (FWHM) of the DCX peak can also be used to judge the quality of the grown epilayer.

4-2-2 PL measurements of the InGaAsP between GaAs on InGaP

The PL spectroscopy is a technique to obtain the relation between the intensity and the wavelength of the emission of radiation. Excess electron-hole pairs are generated when a semiconductor is illuminated by light with photon energy larger than the bandgap. By the processes of excitation, energy transfer and radiative transition, the luminescence was generated from the epilayers. From the wavelength of the PL peak, we can calculate the bandgap of the epilayer or determine which one is the light generating mechanism. The FWHM of the PL peak also give us information about the quality of the epilayers. The LT-PL measurement employed in this study is performed by using a 532 nm, 34 mw solid-state green laser as light source and a PMT detector and all experiment were carried out at 20K.

4-2-3 TEM and STEM for microstructure characterization

TEM and STEM are powerful tools to obtain the information about microstructure of the epilayers. They can help us to understand the relationship between composition, microstructure, defect and interface quality of the epilayer. In our study, we use TEM and SEM to confirm the

existence of the intermixing InGaAsP layer and measure the thickness of the InGaAsP layer grown.



Chapter 5

Results and Discussion

5-1 Modulation of $\text{In}_x\text{Ga}_{1-x}\text{P}$ lattice matched with GaAs

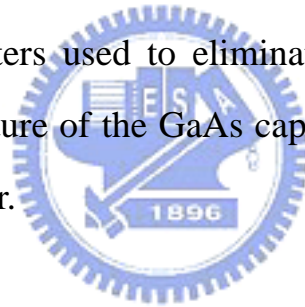
The general growth temperature of the $\text{In}_x\text{Ga}_{1-x}\text{P}$ layer in this experiment was 650°C . The flow rates of TEGa and PH_3 remained constant and the flow rate of TMIIn to was modulate the composition of the $\text{In}_x\text{Ga}_{1-x}\text{P}$ layer. The flow rates of TEGa and PH_3 were 25 sccm and 150 sccm, respectively. Figure 5.1 is the DCX data of Sample *A*, and the flow rate of TMIIn in this case was 54 sccm. The peak of $\text{In}_x\text{Ga}_{1-x}\text{P}$ is broad and is on the left of the GaAs substrate peak. Its FWHM is 141sec. From Fig. 5.1, it is known that the lattice constant of the $\text{In}_x\text{Ga}_{1-x}\text{P}$ layer is larger than that of the GaAs substrate. Therefore the flow rate of TMIIn was reduced to 51 sccm for sample *B*. Figure 5.2 is the DCX data of sample *B*. It could be seen that the peak of $\text{In}_x\text{Ga}_{1-x}\text{P}$ moves closer to the peak of GaAs substrate but still there is a little difference between their lattice constants. The lattice constant of $\text{In}_x\text{Ga}_{1-x}\text{P}$ is still larger than that of GaAs for sample *B*. Figure 5.3 is the DCX of sample *C*. The only difference between samples *B* and *C* is the growth temperature of the $\text{In}_x\text{Ga}_{1-x}\text{P}$ layer. The $\text{In}_x\text{Ga}_{1-x}\text{P}$ layer of sample *C* was grown at 700°C . Although these samples have the same V/III and III/III ratios, the composition of $\text{In}_x\text{Ga}_{1-x}\text{P}$ layers are different from each other. This is because the pyrolysis, desorption and adsorption of precursors vary with temperature. So different growth temperature requires different optimum

V/III and III/III ratio to make $\text{In}_x\text{Ga}_{1-x}\text{P}$ layer lattice matched to GaAs.

After modulation of the TMIn flow rate, the $\text{In}_x\text{Ga}_{1-x}\text{P}$ layer lattice was matched to the GaAs substrate. Figure 5.4 is the DCX of the lattice-matched $\text{In}_x\text{Ga}_{1-x}\text{P}$ layer at the TMIn flow rate = 49.7 sccm. The FWHM of InGaP was 153 sec. The flow rates of the lattice matched InGaP were TMIn: 49.7 sccm, TEGa: 25 sccm, and PH_3 : 150 sccm, respectively.

5-2 Thickness variation of $\text{In}_x\text{Ga}_{1-x}\text{As}_y\text{P}_{1-y}$ at different growth conditions

The growth parameters used to eliminate the $\text{In}_x\text{Ga}_{1-x}\text{As}_y\text{P}_{1-y}$ layer were the growth temperature of the GaAs cap, and PH_3 off time between GaAs cap and InGaP layer.



5-2-1 Dependence of $\text{In}_x\text{Ga}_{1-x}\text{As}_y\text{P}_{1-y}$ layer thickness with growth temperature of the GaAs cap

Figure 5.5 is the schematic diagram of the GaAs/InGaP/GaAs growth process. The only difference of each sample is the growth temperature of the GaAs cap. Figure 5.6(a) ~ Fig. 5.6(d) are the PL intensity *versus* wavelength for these four samples, and the data were summarized in Fig. 5.6(e). These samples are labeled according to their GaAs cap growth temperatures. From Fig. 5.6(a), it can be seen that the peak of $\text{In}_x\text{Ga}_{1-x}\text{As}_y\text{P}_{1-y}$ of sample-650 is the most broaden and intense. We could hardly find the InGaP and GaAs peaks for sample-650. We have already discussed the reason why the PL-peak of $\text{In}_x\text{Ga}_{1-x}\text{As}_y\text{P}_{1-y}$ is

much stronger than those of InGaP and GaAs in Ch.1. In addition, there was an blue-shift of $\text{In}_x\text{Ga}_{1-x}\text{As}_y\text{P}_{1-y}$ peak between sample-650 and sample-625. This was resulted from the composition change of the $\text{In}_x\text{Ga}_{1-x}\text{As}_y\text{P}_{1-y}$ layer due to different GaAs cap growth temperatures. From Fig. 5.6(e), we can find two clear trends of the four samples as the growth temperature of GaAs cap decreases:

- (1) The wavelength of the $\text{In}_x\text{Ga}_{1-x}\text{As}_y\text{P}_{1-y}$ decreases.
- (2) The intensity of the peak belongs to InGaP becomes very intense.

Taking sample-575 as an example, the intensity of $\text{In}_x\text{Ga}_{1-x}\text{As}_y\text{P}_{1-y}$ and InGaP are almost the same. This means that the thickness of $\text{In}_x\text{Ga}_{1-x}\text{As}_y\text{P}_{1-y}$ decreases when lowering the GaAs cap growth temperature. On the other hand, the FWHM of the peak of $\text{In}_x\text{Ga}_{1-x}\text{As}_y\text{P}_{1-y}$ for each sample decreases as GaAs cap growth temperature decreases. We can conclude that not only the thickness of the $\text{In}_x\text{Ga}_{1-x}\text{As}_y\text{P}_{1-y}$ layer was decreased, but also the crystalline quality of the $\text{In}_x\text{Ga}_{1-x}\text{As}_y\text{P}_{1-y}$ was improved as the GaAs cap growth temperature decreased. Undoubtedly, the positions of these peaks corresponding to InGaP and GaAs remained almost the same as GaAs cap growth temperature decreased.

Table 5.1 is the wavelength, FWHM, and the relative-intensity of InGaP to $\text{In}_x\text{Ga}_{1-x}\text{As}_y\text{P}_{1-y}$ for each sample. Obviously, the optimum growth temperature of GaAs cap was 575°C

The existence of the intermixing $\text{In}_x\text{Ga}_{1-x}\text{As}_y\text{P}_{1-y}$ layer is supported by the following TEM and STEM characters.

Figure 5.7 is the TEM image of sample-600. There is an obvious intra-layer between GaAs and InGaP. This is the intermixing

$\text{In}_x\text{Ga}_{1-x}\text{As}_y\text{P}_{1-y}$ layer with non-uniform thickness in the range of 2~5 nm.

Figure 5.8(a) is the HRTEM image of sample-625. Due to the lattice-match between InGaP and GaAs, there are few misfit dislocations across the interface of InGaP/GaAs. Figure 5.8(b) is the depth profile from point *A* to *B* shown in Fig. 5.8(a). From Fig. 5.8(b), there is no obvious step across the interface of GaAs/InGaP due to different material property or TEM sample preparation.

Figure 5.9(a) is the STEM image of sample-625. The $\text{In}_x\text{Ga}_{1-x}\text{As}_y\text{P}_{1-y}$ intermixing layer with thickness about 10 nm is clearly seen in this picture. Figure 5.9(b) is the composition profile across the interface of GaAs/InGaP. Undoubtedly, we can see three regions in Figure 5.9(b). They are GaAs cap, intermixing $\text{In}_x\text{Ga}_{1-x}\text{As}_y\text{P}_{1-y}$, and InGaP, respectively.

5-2-2 $\text{In}_x\text{Ga}_{1-x}\text{As}_y\text{P}_{1-y}$ varies with PH_3 off time between GaAs and InGaP

After determining the optimum T_g of GaAs cap, we inserted different PH_3 off time such as 0 sec, 1 sec, 2 sec, 3 sec and 10 sec during the InGaP and GaAs cap growth. Figure 5.10(a) to Figure 5.10(e) are the PL intensity *verse* wavelength for these five samples.

According to T. Nakano's study [11], the ellipsometric signal change due to phosphorus off purging seemed to reach the plateau after 0.2 sec ~ 1.0 sec interruption at 660°C. This plateau corresponds to the complete desorption of surface P from InGaP. As to our experiment, we grew InGaP at 650°C and grew GaAs cap at 575°C, this would decrease the desorption of P from InGaP surface during PH_3 interruption. From Figs. 5.10(a) ~ 5.10(d), we can find the longer the PH_3 off, the weaker the

relative intensity of $\text{In}_x\text{Ga}_{1-x}\text{As}_y\text{P}_{1-y}$. As shown in Fig. 5.10(d), the relative intensity of $\text{In}_x\text{Ga}_{1-x}\text{As}_y\text{P}_{1-y}$ is much weaker than InGaP. We can draw a conclusion from these results that due to our lower growth temperature of GaAs cap, the desorption of surface P from InGaP during PH_3 interruption was reduced thus we could purge the reactor chamber with a longer PH_3 off time. This would greatly reduce the residual PH_3 and result in thinner $\text{In}_x\text{Ga}_{1-x}\text{As}_y\text{P}_{1-y}$ layer. In addition, there was no obvious shift of $\text{In}_x\text{Ga}_{1-x}\text{As}_y\text{P}_{1-y}$ peak's position. This means the composition of $\text{In}_x\text{Ga}_{1-x}\text{As}_y\text{P}_{1-y}$ layer remained constant with different PH_3 off time at 575°C .

Figure 5.10(e) is the PL intensity *versus* wavelength for the sample with 10 sec PH_3 off. The relative intensity of the $\text{In}_x\text{Ga}_{1-x}\text{As}_y\text{P}_{1-y}$ peak becomes stronger than that of sample with 3 sec PH_3 off. This is resulted from the desorption of surface P from InGaP although the longer the PH_3 off time the fewer the residual PH_3 in the reactor chamber.

From Figs. 5.10(a) ~ 5.10(e), the composition of $\text{In}_x\text{Ga}_{1-x}\text{As}_y\text{P}_{1-y}$ with different PH_3 off time are almost the same. The difference among these samples is the thickness of $\text{In}_x\text{Ga}_{1-x}\text{As}_y\text{P}_{1-y}$ layer. Comparing with Fig. 5.6, we can find the major factor determining the composition of the $\text{In}_x\text{Ga}_{1-x}\text{As}_y\text{P}_{1-y}$ layer is the growth temperature of the GaAs cap.

Figure 5.11(a) is the STEM image of the sample with 0 sec PH_3 off. There is an inserted $\text{In}_x\text{Ga}_{1-x}\text{As}_y\text{P}_{1-y}$ layer with thickness about 5 nm. Figure 5.11(b) is the composition profile across the interface of GaAs and InGaP. There are also three regions in Fig. 5.11(b).

Figure 5.12(a) is the STEM image of the sample with 3 sec PH_3 off. There is no clear $\text{In}_x\text{Ga}_{1-x}\text{As}_y\text{P}_{1-y}$ layer between InGaP and GaAs. This

consists with the data of LT-PL. Figure 5.12(b) is the composition profile across the interface of GaAs/InGaP. There is no obvious composition change across the interface.

Figure 5.13 is the STEM image of the sample with 10 sec PH₃ off. There is also an obvious inserted In_xGa_{1-x}As_yP_{1-y} layer.

5-3 Examination of the InGaP etching stop layer

After determining the growth temperature of the GaAs cap and the PH₃ off time between InGaP and GaAs cap, we grew InGaP layers with different thickness as etching stop layer between GaAs cap and buffer and removed the GaAs layer by mesa etching. The etching rate of our etching solution for GaAs was about 40Å/sec.

The thickness of the InGaP layer of our etching samples were 20 Å, 40 Å, and 80Å, respectively. Figure 5.14 is the etching depth verse etching time for these samples. The sample without InGaP etching stop layer was also etched so as to compare the etching results with other samples. From this sample, we found the etching rate almost remained constant during different etching periods. In addition, for the samples with 20 Å, 40 Å and 80 Å InGaP etching stop layer, the etching stopped at InGaP layer after 16 sec etching process. After 65 sec etching, the sample with 20 Å InGaP layer was penetrated and could not prevent the sub-GaAs layer from being etched. We could conclude that the major etching stop layer are the InGaP not the InGaAsP.

Chapter 6

Conclusions

The desorption of P atoms from InGaP surface at about 650°C was so fast that when we grew GaAs on InGaP, it resulted in arsenic incorporating into InGaP. This incorporation would reduce the bandgap energy. Furthermore, etching selectivity was reduced by the formation of an InGaAsP layer. This required a thinner etching stop layer of InGaP/GaAs material system. By reducing the growth temperature of GaAs cap, the desorption of P atoms from InGaP surface was greatly reduced so the thickness of the spontaneously formed InGaAsP layer was reduced. The LT-PL confirmed with this result. The slower desorption rate of P atoms on the InGaP surface also allowed us to purge the PH₃ in the reactor chamber in a longer time than others' experiments. This would greatly reduce the residual PH₃ in the reactor chamber and reduce the thickness of the formed InGaAsP.

By adopting the optimum condition to grow a thin InGaP etching stop layer between two GaAs layers, we found a 20Å InGaP layer can prevent the sub-GaAs layer from being etched for 45 sec. This greatly reduce the required thickness of InGaP etching layer for InGaP/GaAs system.